Moiré superlattice structures in kicked Bose-Einstein condensates

L. J. O'Riordan, A. C. White, and Th. Busch
Quantum Systems Unit, Okinawa Institute of Science and Technology Graduate University, Onna, Okinawa 904-0495, Japan
(Received 26 November 2015; published 4 February 2016)

Vortex lattices in rapidly rotating Bose-Einstein condensates lead to a periodic modulation of the superfluid density with a triangular symmetry. Here we show that this symmetry can be combined with an external perturbation in order to create superlattice structures with two or more periodicities. Considering a condensate that is kicked by an optical lattice potential, we find the appearance of transient moiré lattice structures, which can be identified using the kinetic energy spectrum.

DOI: 10.1103/PhysRevA.93.023609

I. INTRODUCTION

Ultracold quantum gases have in recent years shown that they can be used as clean, cold, and highly controllable simulators for fundamental effects in solid-state physics. Notable examples of these include strongly correlated lattice systems, Abrikosov vortex states, artificial gauge fields, and electronic spin systems [1]. Here we add another example by showing that superlattice structures can be generated by simply applying an optical pulse to a vortex lattice state. This results in so-called moiré superlattices, which are known to appear in many solid-state [2–4], and even biological [5], systems.

Many of the effects observed in solid-state physics owe their origin to the underlying periodicity of the system. The main effect of the periodicity is the appearance of a band structure in the eigenspectrum, and designing and controlling this band structure is of interest in order to control the physical behavior. In ultracold systems periodicity can be most easily introduced by using optical lattice potentials [6]. Made from a single optical wave vector they provide geometries with perfect and simple periodicity, but combining lasers with two or more differing wave vectors can allow for the creation of superstructures, such as double-well lattices or more exotic geometries [7–10]. Such superlattices can, for example, be used to realize optical gauge fields for neutral atoms [11–14]. Given their experimental accessibility, optical lattices and superlattices allow for studying interesting and often exotic new physics. More recently, spatially periodic systems (supersolids) have also been predicted to appear in the presence of extended interactions [15].

Using optical lattices on condensates, which carry angular momentum, is more complicated, as the rotation of the system is at odds with the (experimentally enforced) stationarity of the lasers that create the optical lattice. Assuming, however, that an optical lattice could be stationary in the corotating frame (see Ref. [16] for an interesting example), several effects have been predicted in recent years. The pinning of vortices by a ramped optical lattice potential [16–18] shows that the vortices follow the lattice maxima, assuming a blue-detuned field. Increasing the optical lattice strength therefore causes the vortex lattice structure to undergo a phase transition from triangular to the geometry of the pinning lattice.

In this work we propose a different approach to combining a rapidly rotating vortex lattice in a Bose-Einstein condensate with an optical lattice: switching the optical lattice on for a very short amount of time (such that only a phase is imprinted) creates a transient phononic excitation pattern of the same periodicity as the optical pulse. The combination of this excitation pattern, and that from the vortex lattice, generates a moiré superlattice pattern in the condensate density [19]. Given the experimental difficulties in rotating the optical lattice with the condensate, the ability to imprint a phase pattern onto the condensate from a pulsed optical potential is much more realizable.

The manuscript is structured as follows. In Sec. II we introduce the system of a Bose-Einstein condensate under rapid rotation and describe the kicking mechanism. The dynamics originating from this are discussed in Sec. III and the observed superstructures are explained using moiré interference theory. We conclude in Sec. IV.

II. MODEL

We consider a single-component Bose-Einstein condensate in a harmonic trap, which in the mean-field limit can be described by the standard Gross-Pitaevskii Hamiltonian

$$H_{\rm GP} = -\frac{\hbar^2}{2m}\nabla^2 + \frac{1}{2}m\omega^2\mathbf{r}^2 + g|\Psi(\mathbf{r},t)|^2. \tag{1}$$

Here ω is the trapping frequency, g describes the strength of the two-particle interaction, and m is the atomic mass. Imposing an external rotation around the z axis and going into the corotating frame leads to a Gross-Pitaevskii equation of the form

$$i\hbar\frac{\partial}{\partial t}\Psi(\mathbf{r},t) = [H_{\rm GP} - \Omega_z L_z]\Psi(\mathbf{r},t), \tag{2}$$

where Ω_z is the rotation frequency around the z axis and $L_z = xp_y - yp_x$ is the angular momentum operator. For a rotational frequency close to the transverse trapping frequency, $\omega_\perp$, the condensate is known to respond by forming a triangular lattice of vortex lines in the x-y plane [20]. Since we are only interested in the effects stemming from the lattice ordering, we will choose the trapping frequency along the z axis, ω_z, to be much larger than the one along the transverse axis, $\omega_\perp$, so that the condensate assumes a pancake-shaped geometry [21]. This allows us to simplify our analysis by neglecting the z dimension ($\mathbf{r} \equiv [x,y]$), and treat the condensate as a two-dimensional system.

In the following we will solve Eq. (1) numerically, using a GPU implemented Fourier split operator method [22]. All simulations will use $N = 4.9 \times 10^5$ atoms of ^{87}Rb, which have an s-wave scattering length of $a_s = 4.76 \times 10^{-9}$m [23].

 ©2016 American Physical Society

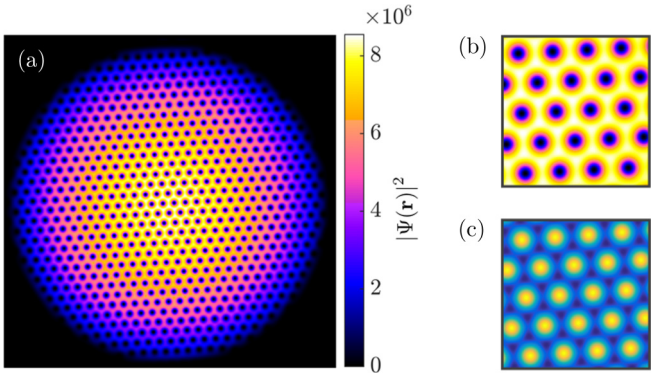

FIG. 1. (a) Vortex lattice ground state in a harmonic trap with $\omega_\perp = 2\pi\ \mathrm{s}^{-1}$ and rotating at $\Omega = 0.995\omega_\perp$. This plot shows a condensate with a diameter of approximately 580 μm; (b) Zoom in of vortex lattice at central density; (c) Optical lattice potential with a periodicity matching that of the vortex lattice.

The trapping frequency will be fixed at $\omega_\perp = 2\pi\ \mathrm{s}^{-1}$, the rotation frequency at $\Omega = 0.995\omega_\perp$, and the effective two-dimensional interaction strength is given by

$$g_{2\mathrm{d}} = \frac{4\pi\hbar^2 a_s N}{m}\sqrt{\frac{m\omega_z}{2\pi\hbar}}. \tag{3}$$

The numerically calculated ground state for the above set of parameters is shown in Fig. 1 and it can be characterized by the filling factor (or filling fraction) $\nu = N/N_v$, i.e., the ratio of atoms to vortices [21]. For the chosen parameters, the number of vortices within the visible density region is approximately 600, giving a filling factor of $\nu \approx 800$. This places the system within the mean-field quantum Hall regime, and therefore a description using Gross-Pitaevskii theory is adequate [24]. The vortex lattice is highly periodic and the triangular lattice vectors in $\mathbf{r}$ space are given by $\mathbf{a}_1 = a_v\{1,0\}$ and $\mathbf{a}_2 = a_v\{-1/2,\sqrt{3}/2\}$, where a_v is the distance between vortex cores. For our analysis we chose to ignore vortices close to the condensate edge, as the distortions in the vortex lattice mean the system can no longer be modelled as a homogeneous arrangement of vortices. The reciprocal ($\mathbf{k}$-space) lattice vectors corresponding to the given $\mathbf{r}$-space vectors are $\mathbf{b}_1 = 4\pi/(\sqrt{3}a_v)\{\sqrt{3}/2,1/2\}$ and $\mathbf{b}_2 = (4\pi/(\sqrt{3}a_v))\{0,1\}$.

To create a perturbation the condensate is *kicked* by switching on an additional optical potential for a period of time that is much shorter than the rotation period of the Abrikosov lattice ($\tau_{\mathrm{kick}} = 10^{-5}$s). The vortex lattice is therefore effectively stationary during the kick. In order to create effects based on periodicity, we chose the optical potential to have the form of a standing lattice, which has the same geometry as the Abrikosov lattice, however not necessarily the same orientation [see Fig. 1(c)]. To construct such a lattice potential, V_{opt}, we sum counterpropagating laser beams to get

$$V_{\mathrm{opt}} = V_0 \sum_j \cos^2[\mathbf{k}_j \cdot \mathbf{r}], \tag{4}$$

where V_0 is the amplitude of the optical lattice potential, and $j = \{0,1,2,\ldots\}$ is the index of each respective laser with a differing $\mathbf{k}$-space wave vector. The triangular structure of the vortex lattice can then be matched by choosing wave vectors corresponding to the optical potential that follow the vortex lattice vectors $\mathbf{b}_{1,2}$ and adding a third wave vector with $\mathbf{k}_3 = 4\pi/(\sqrt{3}a_o)\{\sqrt{3}/2, -1/2\}$. Note that these wave vectors have a lattice constant a_o, which is based on the optical intensity in order to compare with the vortex lattice later. However, as the intervortex separation in atomic Bose-Einstein condensates is large, one needs to employ optical lattices with wavelengths on the order of tens of μm [25,26]. For short kicks, and amplitudes on the order of $10^{-2}\mu$, where μ is the chemical potential of the system, the effect of the kick is limited to a phase imprint on the condensates wave function [27], which subsequently leads to the development of a flow originating from the position of each maximum of the optical potential. In the following we will show that this in turn leads to well-defined phonon interferences, which, when overlaid on the periodically arranged vortex cores, gives rise to the appearance of moiré superlattice structures [28] in the condensate density. While in many solid-state systems, for example graphene on hexagonal boron nitride [2], the moiré structures are static superstructures, in our case they are dynamical and appear at well-defined intervals.

To identify the moiré lattices, we perform a spectral decomposition of the kinetic energy of the condensate [29–31]. For this we write the wave function in terms of its density, $\rho(\mathbf{r},t)$, and phase, $S(\mathbf{r},t)$, as $\Psi(\mathbf{r},t) = \sqrt{\rho(\mathbf{r},t)}\exp[\mathrm{i}S(\mathbf{r},t)]$, and obtain from the kinetic energy term in the Gross-Pitaevskii energy functional

$$E_{\mathrm{kqp}} = \int d\mathbf{r}\left(\frac{\hbar^2}{2m}|\nabla\sqrt{\rho(\mathbf{r},t)}|^2 + \frac{m}{2}|\sqrt{\rho(\mathbf{r},t)}\mathbf{v}(\mathbf{r},t)|^2\right). \tag{5}$$

The first term in this expression can be interpreted as the quantum pressure term, and the second describes the kinetic energy. We denote the density weighted velocity field as $\mathbf{u}(\mathbf{r},t) = \sqrt{\rho(\mathbf{r},t)}\mathbf{v}(\mathbf{r},t)$, and further decompose it into compressible, $\mathbf{u}^c(\mathbf{r},t)$, and incompressible, $\mathbf{u}^i(\mathbf{r},t)$ terms

$$\mathbf{u}(\mathbf{r},t) = \mathbf{u}^c(\mathbf{r},t) + \mathbf{u}^i(\mathbf{r},t), \tag{6}$$

defined by $\nabla \times \mathbf{u}^c(\mathbf{r},t) = 0$, and $\nabla \cdot \mathbf{u}^i(\mathbf{r},t) = 0$. This decomposition allows the energy contribution from vortex cores (incompressible) and phonon modes (compressible) to be separated [33]. The compressible and incompressible kinetic energy spectra, $E^{c,i}(k)$, are calculated by averaging over shells in $\mathbf{k}$ space as [31]

$$E^{c,i}(k) = \frac{mk}{2}\sum_{j\in\mathbf{r}}\int_0^{2\pi} d\phi_k \frac{|\mathcal{U}_j^{c,i}(\mathbf{k},t)|^2}{s_k}, \tag{7}$$

where

$$\mathcal{U}_j^{c,i}(\mathbf{k},t) = \int d^2\mathbf{r} e^{-i(\mathbf{k}\cdot\mathbf{r})} u_j^{c,i}(\mathbf{r},t). \tag{8}$$

Here the $u_j^{c,i}(\mathbf{r},t)$ are the values of the position-space kinetic energy components in the specified shell, ϕ_k is the polar angle, and s_k represents the number of elements in the chosen shell.

III. DYNAMICS FOLLOWING A KICK

A. Nonrotating condensate

To understand the effect kicking has on a condensate carrying a vortex lattice, we will first briefly examine the situation where the vortex lattice is absent, i.e., where there is no external rotation. In order to compare this situation with a rapidly rotating condensate, we adjust the trapping frequency in this section such that the background densities match.

For a stationary (nonkicked) condensate the kinetic energy spectrum is constant during time evolution and a kick leads to the appearance of new, time-varying components. To observe this we numerically evolve the system by setting $V(\mathbf{r},t) = V_{\text{ext}}(\mathbf{r}) + V_{\text{opt}}(\mathbf{r},t)$, where the time-dependent optical potential is only active for $\tau = 10^{-5}$s of the simulation time, and examine the compressible kinetic energy spectrum following the kick (see Fig. 2). Unsurprisingly, the spectrum is dominated by a peak corresponding to the wave vector associated with the optical potential at $k = 4\pi/(\sqrt{3}a_o)$, and several smaller ones corresponding to its higher harmonics and higher harmonics of next-nearest-neighbor components of the lattice. As no rotation is created by the imparted phonon modes, the incompressible energy is negligible and we will therefore restrict our analysis to the compressible part of the spectrum.

The evolution of the main peak in the compressible kinetic energy spectrum during the first 250 ms after the kick is shown in Fig. 3(a). It initially oscillates in and out of existence and eventually disperses over a wide range of wave numbers. Snapshots of the density evolution are shown in Fig. 3(b), which clearly show that the oscillations correspond to the existence of a transient lattice pattern with several revivals, which has the same underlying structure as the optical potential. In fact, the lattice pattern is best formed whenever

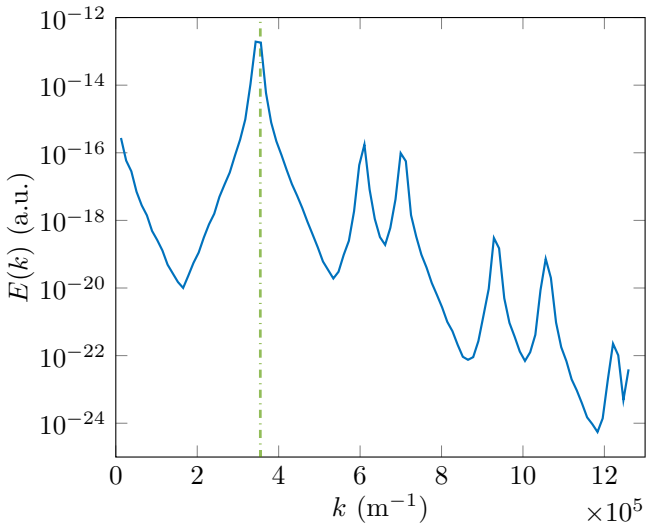

FIG. 2. Compressible energy spectrum of a nonrotating condensate directly following a kick. A peak at $k = 4\pi/(\sqrt{3}a_o)$ can be seen, which corresponds to the lattice spacing, a_o (indicated by the dashed line), and the smaller, higher-energy peaks can be attributed to higher harmonics between nearest and next-nearest neighbours.

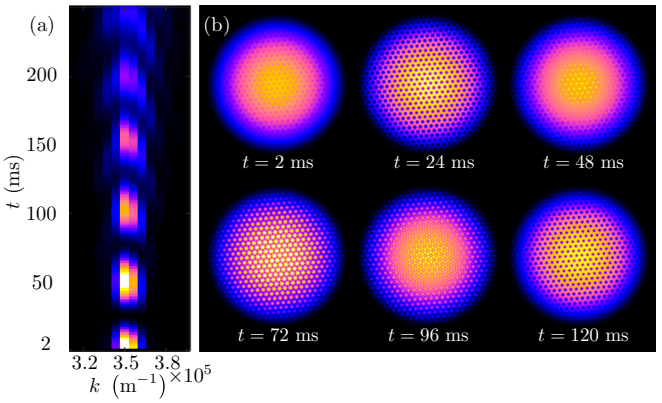

FIG. 3. (a) Main peak of the compressible kinetic energy spectrum for a kicking strength of $V_0 \approx 1.35 \times 10^{-2}\mu$. It can be seen to revive, and eventually disperse, over a wide range of wave numbers. (b) Condensate densities at several times during the evolution. A pattern matching the optical potential can be observed to appear and disappear several times over the course of the evolution.

the main peak in the kinetic energy spectrum goes to zero, i.e., when the imprinted kinetic energy has been converted into density modulations. The period of the oscillations can be related to the speed of sound divided by the lattice constant and therefore the appearance of the lattice can be attributed to phonon interferences.

B. Rapidly rotating condensate

Kicking a condensate carrying an Abrikosov vortex lattice with the above optical lattice gives an additional parameter, θ_Δ, which describes the orientation of the imprinted phonon lattice angle relative to the vortex lattice. For simplicity, we assume that the vortex and optical potential lattices have the same lattice constant, $a_v = a_o = a$ (see below for a discussion of the incommensurate case), which means that symmetry allows us to restrict the angle to $\theta_\Delta \in [0,\pi/3]$. We will show in the following that adjusting θ_Δ leads to the appearance of different, transient superstructures in the condensate density.

If $\theta_\Delta = 0$ [see Fig. 4(a)] the kicking imparts kinetic energy at wave numbers that are already well defined in the lattice. This leads to an expansion and contraction of the vortex cores in density only, and no significant change to the compressible kinetic energy spectrum.

However, if the angle between both lattices is finite, superlattice structures appear after a short time [see Figs. 4(b)–4(d)], which have a structure cell size that decreases for increasing values of $\theta_\Delta \in [0,\pi/6]$ and increases for larger values until the misalignment angle reaches the lattice symmetry point again at $\theta_\Delta = \pi/3$. These structures are transient and several revivals can be observed before the condensate settles back into the vortex lattice structure with an increase in the background wave-number spread, as expected based on kicking the nonrotating condensate. An example of this for a fixed angle is shown in Fig. 5.

To explain the interference patterns observed for misaligning the optical and the vortex lattice, we employ moiré interference theory [32]. Moiré patterns are known to appear when two periodic structures are overlaid while slightly misaligned

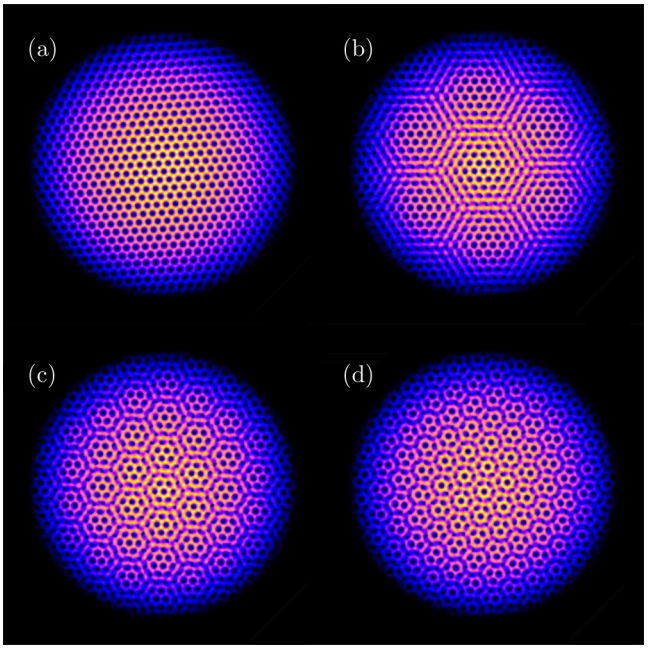

FIG. 4. Condensate density at $t = 1.4 \times 10^{-2}$ s for several optical lattice rotation angles. The cell size of the superlattice structures can be seen to shrink as the angle is increased. The angles for the examples shown are (*a*) $\theta_\Delta = 0$, (*b*) $\theta_\Delta = 2\pi/45$, (*c*) $\theta_\Delta = 4\pi/45$, (*d*) $\theta_\Delta = 2\pi/15$.

to each other and can be calculated from the reciprocal lattice vectors. In all generality, any choice of equidistantly separated reciprocal lattice vectors be parameterized as

$$\mathbf{g}_l = g_0\left[\sin\left(\frac{2\pi l}{\alpha}+\theta\right), \quad \cos\left(\frac{2\pi l}{\alpha}+\theta\right)\right], \tag{9}$$

where α describes the rotational symmetry of the lattice, l labels the vector direction on the unit circle, θ is the angle with respect to a chosen coordinate system and g_0 is the reciprocal lattice constant. For our commensurate and triangular lattices we have $g_0 = 4\pi/(\sqrt{3}a)$, $\alpha = 6$ and the vector directions are

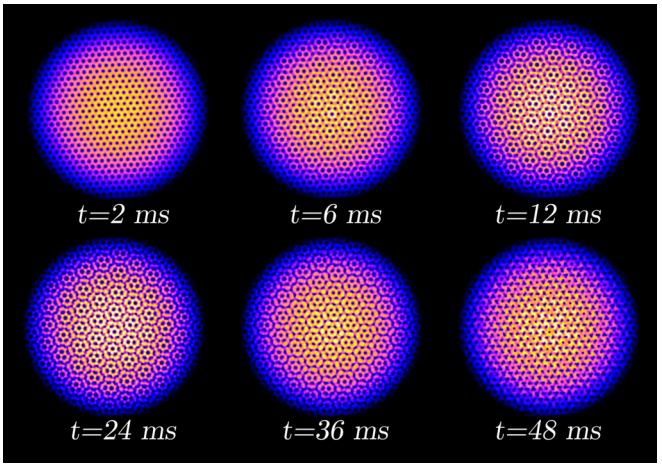

FIG. 5. Condensate density after receiving a kick with $\theta_\Delta = \pi/9$. The appearance and disappearance of a moiré structure with wavelength $\lambda_M \approx 2.9a$ over a timescale of about 50 ms can be seen.

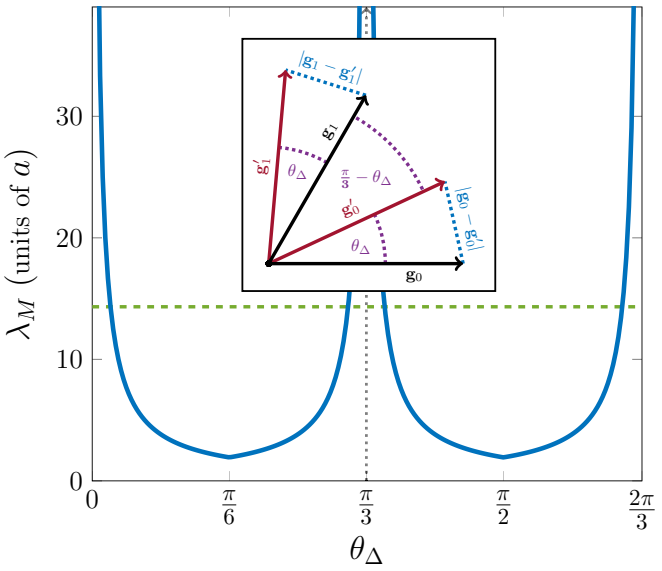

FIG. 6. Size of the resulting moiré superstructures as a function of the relative angle between the vortex and optical lattice. The dashed green line indicates the condensate radius. Inset: The different vectors in **k** space of the two lattices, with the optical lattice rotated by an angle θ_Δ. The $\mathbf{g}_{ll'} = |\mathbf{g}_l - \mathbf{g}'_l|$ vectors defining the dominant moiré wavelength are those for which the enclosed angle is smallest.

$l = [0 \ldots \alpha - 1]$. As only the relative misalignment between the vortex and the phonon lattice matters, we choose $\theta = 0$ for the vortex lattice and $\theta = \theta_\Delta$ for the optical potential alignment. All possible wavelengths that can appear in an interference pattern between two such lattices in real space are then given by

$$\lambda_{ll'} = \frac{\lambda_0}{|\mathbf{g}_{ll'}|}, \tag{10}$$

where $\mathbf{g}_{ll'} = \mathbf{g}_l^{\mathrm{V}} - \mathbf{g}_{l'}^{\mathrm{P}}$, and $\lambda_0 = 4\pi/\sqrt{3}$ for our commensurate triangular lattices. One can see from Fig. 5 that a pattern matching the longest wavelength, $\lambda_M = \max[\lambda_{ll'}] \approx 2.9a$, appears around $t = 24$ ms and is clearly the most visible one. While patterns with shorter wavelength exist, they are harder to discern in our system and we therefore concentrate on the lowest wave number in the following.

In **k** space the shortest $|\mathbf{g}_{ll'}|$ corresponds to adjacent wave vectors with the smallest θ_Δ between them (see inset in Fig. 6). Due to the symmetry of the lattices the most visible structures are therefore given by $\lambda_M = \lambda_{00}$ for $\theta_\Delta \in [0,\pi/6]$ and $\lambda_M = \lambda_{01}$ for $\theta_\Delta \in [\pi/6,\pi/3]$ (see inset of Fig. 6). While this symmetry assumption no longer holds strictly true after the system has been kicked, it is still fulfilled to a very good approximation during the initial dynamics. We can then obtain the wavelength of the dominating moiré structure as [2,5]

$$\lambda_M = \frac{a}{2\sin(\eta/2)}, \tag{11}$$

where $\eta = \min\{\theta_\Delta, \frac{\pi}{3} - \theta_\Delta\}$ (see Fig. 6). These superstructures become observable when the wavelength becomes smaller than the radius of the condensate, which is $\lambda_M \approx 11a$ and which corresponds to an angle $\theta_\Delta \approx \pi/36$. One can see from Fig. 6 that once the relative angle is increased beyond

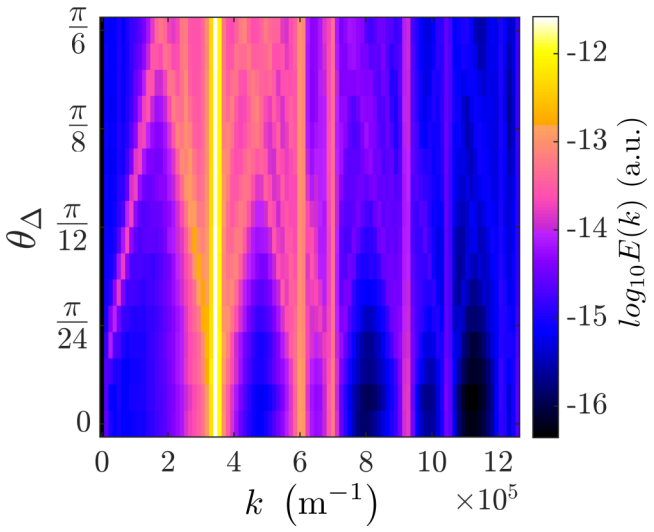

FIG. 7. Compressible kinetic energy spectrum as a function of θ_Δ. All values are time averaged over an interval $t = 0$ s to $t = 1$ s. The moiré peak corresponding to the lowest wave number can be seen shifting to larger values for increasing angles and similar behavior is visible for the higher-order components.

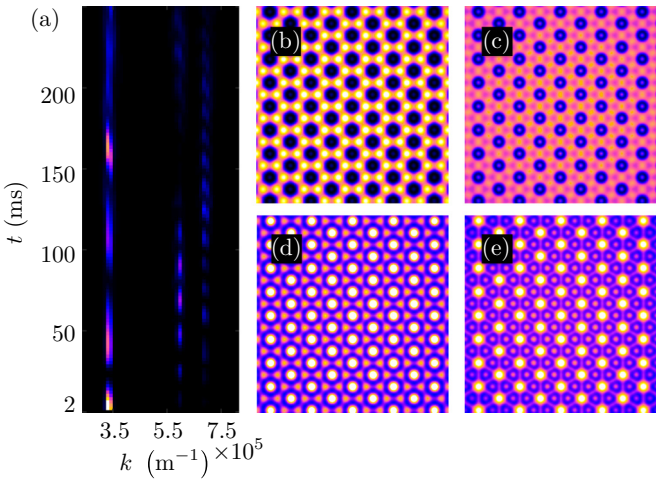

FIG. 8. (a) For a kicking strength of $V_0 = 5.4 \times 10^{-2}\mu$ for a nonrotating condensate higher-order modes become non-negligible contributions to the compressible kinetic energy spectrum. This leads to a variety of different density structures, with some closeups shown for (b) 24 ms, (c) 36 ms, (d) 56 ms, and (e) 88 ms. Note that the larger structures in these plots are given by the optical lattice constant, which sets the scale.

this value the structure sizes shrink to a minimum value at the point of complete misalignment, $\theta_\Delta = \pi/6$, giving $\lambda_M \approx 1.93\,a$, and increase again up to the point of symmetry. Beyond this point the whole behavior starts over, due to the symmetry of the lattice. Note that in principle the above procedure can be carried out for square or other optical lattice geometries.

The appearance of the moiré vector in k space can be confirmed from the numerical simulations by looking at the compressible kinetic energy spectra, which we display in Fig. 7.

Apart from the dominant peaks corresponding to the underlying triangular geometry of the Abrikosov lattice, which are independent of θ_Δ (straight lines in Fig. 7), a number of additional peaks appear. Their position is a function of the misalignment angle and the lowest wave number that appears increases its value with increasing Δ_θ. This is consistent with the moiré model and the appearance of density structures of differing size. Furthermore, a symmetric repeat of this structure about the $\theta_\Delta = \pi/6$ point is also visible, which corresponds to the $\pi/3 - \theta_\Delta$ lattice vector component. The minimum wavelength observed agrees with the theoretically determined minimum value of $\lambda_M \approx 1.93\,a$ and all other values over the range of observed angles. Note that for the higher harmonics at larger wave numbers similar behavior exists and is also covered by the moiré model.

Let us briefly discuss what happens for stronger kicking, or when the two lattices are noncommensurate. In the above the strength of the kicking pulse was chosen such that its perturbation only leads to a phase imprinting [27,34], with minimal change to the initial density. If one increases the kicking intensity the situation becomes quite different and one can see from Fig. 8(a) that higher-order wave numbers become more strongly excited. This, in turn, leads to modulations of the condensate density at shorter wavelength and an example is shown in Figs. 8(b)–8(e). However, as for fully realistic experimental situations it is necessary to consider the heating of the condensates due to the disturbance once the kicking becomes stronger, we restrict this investigation to low-intensity pulses.

A situation where the optical and the vortex lattice have different lattice constants can be imagined to appear naturally due to experimental uncertainties. Defining $a_o = a_v(1+\epsilon)$ the expression in Eq. (10) can be calculated to be

$$\lambda_M = \frac{a_v(1+\epsilon)}{\sqrt{2(1+\epsilon)(1-\cos\theta)+\epsilon^2}}, \tag{12}$$

which reduces to Eq. (11) for $\epsilon = 0$. Evaluating this expression shows that the largest moiré wavelength changes slightly for small values of ϵ, but it remains distinct enough from the underlying wave vectors to stay visible in the evolution. This ensures that the system examined here is experimentally realistic.

IV. CONCLUSIONS

We have examined the evolution of the density and kinetic energy spectra of a rapidly rotating Bose-Einstein condensate following a kick from a periodic optical potential. The kick was chosen to be short enough to effectively see a stationary condensate and weak enough to only lead to phase imprinting. The presence of an inhomogeneous phase consequently leads to the appearance of phonon modes, which coherently interfere at certain times to form a lattice in the condensate density. This lattice, and the existing lattice from the Abrikosov arrangement of the vortices, were shown to interfere and give rise to so-called moiré structures. As the system is dynamical, these structures are temporary and reappear for a number of times before the spreading of the wave numbers leads to the effect washing out.

As the patterns that are created by the lattice interference are of much larger size than the underlying vortex lattice, the above mechanism of moiré interference can have an interesting application as a microscope. In our example the vortex lattice modifies the density on the scale of the healing length, which is not resolvable without time-of-flight data. However, the moiré structures, which are a direct consequence of the lattice structure, are several times larger and might even be visible through direct imaging at the right time. This process could be applied to other density perturbations as well, for example higher-order dark soliton trains. It would also be interesting to apply it to other vortex lattice configurations [35] or vortices in the turbulent regime.

ACKNOWLEDGMENTS

The authors acknowledge support for this work from the Okinawa Institute of Science and Technology Graduate University. We are grateful to JSPS for partial support from Grant-in-Aid for Scientific Research (Grant No. 26400422).

[1] I. Bloch, J. Dalibard, and W. Zwerger, Rev. Mod. Phys. **80**, 885 (2008).
[2] M. Yankowitz, J. Xue, D. Cormode, J. D. Sanchez-Yamagishi, K. Watanabe, T. Taniguchi, P. Jarillo-Herrero, P. Jacquod, and B. J. LeRoy, Nat. Phys. **8**, 382 (2012).
[3] J. Y. Romanova, E. V. Demidov, L. G. Mourokh, and Y. A. Romanov, J. Phys.: Condens. Matter **23**, 305801 (2011).
[4] X. Li, F. Zhang, Q. Niu, and J. Feng, Sci. Rep. **4**, 6397 (2014).
[5] H. T. Blair, A. C. Welday, and K. Zhang, J. Neurosci. **27**, 3211 (2007).
[6] I. Bloch, J. Dalibard, and S. Nascimbène, Nat. Phys. **8**, 267 (2012).
[7] M. Anderlini, J. Sebby-Strabley, J. Kruse, J. V. Porto, and Wm. D. Phillips, J. Phys. B **39**, S199 (2006).
[8] P. Barmettler, A. M. Rey, E. Demler, M. D. Lukin, I. Bloch, and V. Gritsev, Phys. Rev. A **78**, 012330 (2008).
[9] C. Becker, P. Soltan-Panahi, J. Kronjäger, S. Dörscher, K. Bongs, and K. Sengstock, New J. Phys. **12**, 065025 (2010).
[10] G. B. Jo, J. Guzman, C. K. Thomas, P. Hosur, A. Vishwanath, and D. M. Stamper-Kurn, Phys. Rev. Lett. **108**, 045305 (2012).
[11] M. Aidelsburger, M. Atala, S. Nascimbène, S. Trotzky, Y. A. Chen, and I. Bloch, Phys. Rev. Lett. **107**, 255301 (2011).
[12] F. Gerbier and J. Dalibard, New J. Phys. **12**, 033007 (2010).
[13] I. M. Georgescu, S. Ashhab, and F. Nori, Rev. Mod. Phys. **86**, 153 (2014).
[14] Y. J. Lin, R. L. Compton, K. Jiménez-García, J. V. Porto, and I. B. Spielman, Nature (London) **462**, 628 (2009).
[15] M. Boninsegni and N. V. Prokof'ev, Rev. Mod. Phys. **84**, 759 (2012).
[16] S. Tung, V. Schweikhard, and E. A. Cornell, Phys. Rev. Lett. **97**, 240402 (2006).
[17] J. W. Reijnders and R. A. Duine, Phys. Rev. Lett. **93**, 060401 (2004).
[18] T. Mithun, K. Porsezian, and B. Dey, Phys. Rev. A **89**, 053625 (2014).
[19] I. Amidror, *The Theory of the Moiré Phenomenon: Periodic Layers*, Vol. 1 (Springer-Verlag, Berlin, 2009).
[20] J. R. Abo-Shaeer, C. Raman, J. M. Vogels, and W. Ketterle, Science **292**, 476 (2001).
[21] A. Fetter, Rev. Mod. Phys. **81**, 647 (2009).
[22] To achieve sufficient resolution in **k** space we chose a system size of minimum of $2^{10} \times 2^{10}$ grid points. To obtain results within a reasonable time we made use of a GPU implemented Fourier split-operator method that takes advantage of the parallelizable nature of the required operations (FFT, Hadamard product, summation). All of the simulations described use code developed and released under the title GPUE, which is available under the BSD license at https://github.com/mlxd/GPUE
[23] J. L. Roberts, N. R. Claussen, J. P. Burke, Jr., C. H. Greene, E. A. Cornell, and C. E. Wieman, Phys. Rev. Lett. **81**, 5109 (1998).
[24] V. Schweikhard, I. Coddington, P. Engels, V. P. Mogendorff, and E. A. Cornell, Phys. Rev. Lett. **92**, 040404 (2004).
[25] L. Fallani, C. Fort, J. Lye, and M. Inguscio, Opt. Express **13**, 4303 (2005).
[26] R. A. Williams, J. D. Pillet, S. Al-Assam, B. Fletcher, M. Shotter, and C. J. Foot, Opt. Express **16**, 16977 (2008).
[27] Ł. Dobrek, M. Gajda, M. Lewenstein, K. Sengstock, G. Birkl, and W. Ertmer, Phys. Rev. A **60**, R3381 (1999).
[28] Y. Murata, V. Petrova, B. B. Kappes, A. Ebnonnasir, I. Petrov, Y. H. Xie, C. V. Ciobanu, and S. Kodambaka, ACS Nano **4**, 6509 (2010)
[29] C. Nore, M. Abid, and M. E. Brachet, Phys. Fluids **9**, 2644 (1997).
[30] C. Nore, M. Abid, and M. E. Brachet, Phys. Rev. Lett. **78**, 3896 (1997).
[31] A. S. Bradley and B. P. Anderson, Phys. Rev. X **2**, 041001 (2012).
[32] K. Hermann, J. Phys.: Condens. Matter **24**, 314210 (2012).
[33] T. L. Horng, C. H. Hsueh, S. W. Su, Y. M. Kao, and S. C. Gou, Phys. Rev. A **80**, 023618 (2009).
[34] J. Denschlag, J. E. Simsarian, D. L. Feder, C. W. Clark, L. A. Collins, J. Cubizolles, L. Deng, E. W. Hagley, K. Helmerson, W. P. Reinhardt, S. L. Rolston, B. I. Schneider, and W. D. Phillips, Science **287**, 97 (2000)
[35] S. McEndoo and Th. Busch, Phys. Rev. A **79**, 053616 (2009).